NANOMATERIALS

Supertwisted spirals of layered materials enabled by growth on non-Euclidean surfaces

Yuzhou Zhao[1], Chenyu Zhang[2], Daniel D. Kohler[1], Jason M. Scheeler[1], John C. Wright[1], Paul M. Voyles[2], Song Jin[1]*

Euclidean geometry is the fundamental mathematical framework of classical crystallography. Traditionally, layered materials are grown on flat substrates; growing Euclidean crystals on non-Euclidean surfaces has rarely been studied. We present a general model describing the growth of layered materials with screw-dislocation spirals on non-Euclidean surfaces and show that it leads to continuously twisted multilayer superstructures. This model is experimentally demonstrated by growing supertwisted spirals of tungsten disulfide (WS_2) and tungsten diselenide (WSe_2) draped over nanoparticles near the centers of spirals. Microscopic structural analysis shows that the crystal lattice twist is consistent with the geometric twist of the layers, leading to moiré superlattices between the atomic layers.

Two-dimensional (2D) van der Waals (vdW) layered materials offer an ideal platform for creating artificial structures with new properties by vertically stacking different layers (*1*–*3*). Tuning the twist angles between stacked bilayers results in the formation of moiré patterns and the manipulation of electronic states, leading to observations of quantum phenomena, including unconventional superconductivity (*4*), moiré excitons (*5*–*8*), and tunable Mott insulators (*9*, *10*). Twisted structures have been fabricated by elaborate mechanical stacking of different layers in a one-off and low-throughput fashion (*3*–*10*). Beyond twisted bilayers, recent theoretical studies also suggest interesting phenomena in continuously twisted multilayer structures that are termed "3D twistronics" (*11*–*13*). Even though the Eshelby twist (*14*) was recently demonstrated on screw-dislocated nanowires of layered germanium(II) sulfide (*15*, *16*), the amount of twist per layer is quite minute for large-area 2D structures because the Eshelby twist angle is inversely proportional to the lateral cross-sectional area. A different approach is thus desired to directly grow twisted 2D materials and control the interlayer twisting.

Euclidean space provides the mathematical framework for classical crystallography (*17*). Basic concepts such as crystal lattice and symmetry operations are defined in Euclidean space, which shape our understanding of the physical world in which we live. Intuitively, flat substrates with Euclidean surfaces are used in the growth and mechanical stacking of 2D materials. By contrast, non-Euclidean spaces refer to curved geometrical spaces where the parallel postulate is false (*18*) and the geometric transformations originally defined in Euclidean geometry, such as translation and rotation, have different consequences. Because translational symmetry is the central symmetry of crystal lattice, those differences could influence the crystal growth process in non-Euclidean spaces, resulting in exotic new structures. Here, we propose a growth model of screw-dislocated spirals of 2D materials on non-Euclidean surfaces that predicts continuously twisted superstructures in which the large and variable twist angle is exclusively determined by the shape of the non-Euclidean surface and experimentally demonstrate this model on metal dichalcogenides (MX_2).

2D materials typically grow through a layer-by-layer growth mechanism to yield aligned crystal layers. However, owing to the weak vdW interaction between layers, layer-by-layer growth can infrequently generate a small fraction of randomly twisted layers as by-products (*19*, *20*), but the theoretical basis for controlling the twisting from one layer to the next during direct growth is lacking. By contrast, the screw dislocation–driven growth mechanism creates "new layers" by propagating the self-perpetuating growth steps generated by screw dislocations (*21*–*23*). Screw dislocation is a line defect that shears part of the crystal lattice along a specific direction. In layered materials, the shear typically happens along the out-of-plane direction and connects layers into one continuous layer, like in a parking ramp (movie S1). When its stress effect [i.e., Eshelby twist (*14*)] is negligible, an ideal screw dislocation preserves the orientation of each layer owing to the global translational symmetry of the crystal. This generates an aligned spiral shape of edges that are all parallel (Fig. 1A). Such a shape has been observed in many 2D materials such as hexagonal spirals in graphene and hexagonal boron nitride (*24*, *25*) as well as in triangular or hexagonal spirals in metal chalcogenides, such as WSe_2 (*22*), MoS_2 (*26*), WS_2 (*27*), and Bi_2Se_3 (*28*).

Geometry provides a fundamental reason behind the aligned shapes of crystals even in the presence of screw dislocations: The translational symmetry of crystal lattice follows Euclidean geometry. This dictates two basic geometric properties for the shape of a single crystal: First, the angle between two adjacent edges is fixed by their crystallographic indices (*17*), and second, the sum of the measures of the exterior angles is 360° for any convex polygon formed by edges in Euclidean geometry (*18*). These properties can explain the fact that screw-dislocated MX_2 often grow in triangular spiral shapes with aligned edges (Fig. 1A_1 and fig. S1A) (*22*, *26*, *27*). The threefold crystal structure of monolayer MX_2 causes its equilateral triangular shape (*29*) and the 120° exterior angles. Even when a screw dislocation is introduced, the translational symmetry of the crystal is still mostly conserved. In the normal spiral shape, for each period of three consecutive edges, the sum of the exterior angles is 120° + 120° + 120° = 360°, which means that the new and old edges must be parallel. In a typical crystal growth process, the Euclidean geometry of flat substrates matches the Euclidean nature of lattice; as a result, all layer edges are aligned in these dislocated spirals.

By contrast, the sum of the measures of the exterior angles of a polygon is not 360° in non-Euclidean geometry (*18*). Because such a property is not compatible with the Euclidean nature of crystals, tiling Euclidean crystal lattices in non-Euclidean spaces leads to new consequences. We specifically consider growing 2D vdW crystals on conical surfaces, because conical surfaces are "developable surfaces" that are locally isometric to plane, which means that they can be flattened onto a plane without distortion (*30*). Conversely, one can bend and fold a plane into a cone without distortion: As illustrated in Fig. 1B, one must shear half of the plane along the radius and overlap a sector defined by an angle of α. Unfolding the cone surface then results in a circular sector with the angle of 360° – α, which means that on the cone surface, the angle measure of any "full circle" containing the apex is a constant 360° – α and thus the sum of the measures of the exterior angles of any polygon surrounding the apex is also 360° – α. The geometry of the conical surface is non-Euclidean in the sense that it has a singularity at its apex (*30*), which changes the rules of angles on the conical surfaces and influences the translational and rotational operations. If one tries to draw a simple triangular spiral on such a surface by drawing edges by the angles, for every period, the new edge will twist by an angle of α relative to the edge in the last period (Fig. 1A_2), owing to the non-Euclidean geometry of the cone surface.

[1]Department of Chemistry, University of Wisconsin–Madison, Madison, WI 53706, USA. [2]Department of Materials Science and Engineering, University of Wisconsin–Madison, Madison, WI 53706, USA.
*Corresponding author. Email: jin@chem.wisc.edu

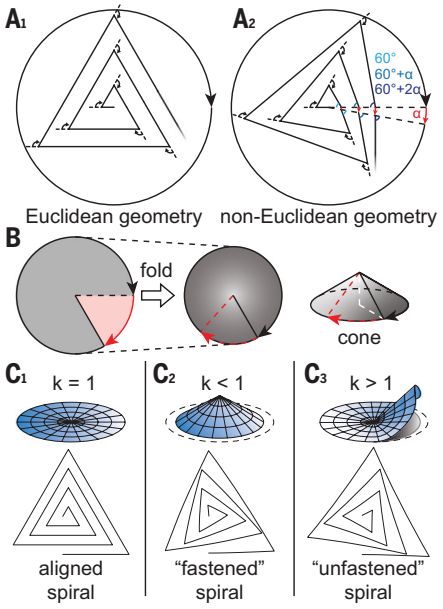

Fig. 1. Triangular dislocation spiral on Euclidean and non-Euclidean surfaces illustrating the twisting process. (**A_1**) For a triangular spiral on a Euclidean surface, at each vertex, the edge direction changes 120°; thus, after three vertices, it turns 360°, which makes the edge parallel to its original orientation. (**A_2**) For a triangular spiral on an unfolded non-Euclidean cone surface, after every three vertices, the edge goes across the dashed line once, so it needs to turn an extra angle of α to keep itself straight. (**B**) A cone can be folded from a circle by cutting along the radius and folding with an angle. (**C_1**) Euclidean surface (k = 1) and a corresponding aligned spiral with no twist. (**C_2**) Non-Euclidean cone surface (k < 1) and a corresponding fastened spiral with a positive twist, which forms a right-handed twisting superstructure. (**C_3**) Non-Euclidean hyperbolic cone surface (k > 1) and a corresponding unfastened spiral with a negative twist, which forms a left-handed twisting superstructure. In (C), all screw dislocations are right-handed, and k is defined as the ratio between the angular period of the specific surface to the period of a Euclidean circle.

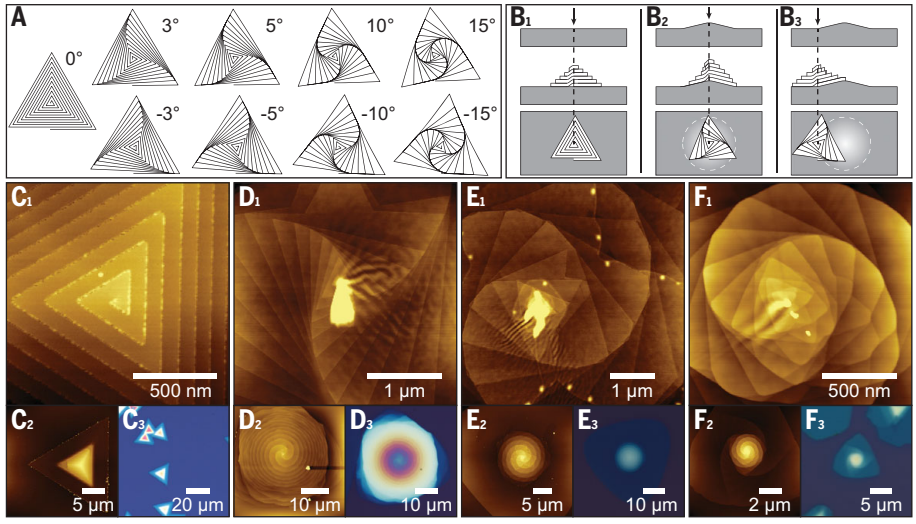

Fig. 2. Simulation and experimental demonstration of supertwisted spirals on non-Euclidean surfaces. (**A**) Simulated superstructures of triangular dislocation spirals with increasing positive or negative twist angles. (**B_1**) A flat substrate surface yields aligned spirals. (**B_2**) A protruded substrate where the center of the screw dislocation sits on top of a protrusion results in a fastened supertwisted spiral. (**B_3**) A protruded substrate where the center of the screw dislocation sits on the edge of a protrusion leads to an unfastened supertwisted spiral. (**C**) AFM (C_1 and C_2) and optical (C_3) images of aligned WS_2 spirals grown on flat SiO_2/Si substrate. (**D** to **F**) AFM (D_1, D_2, E_1, E_2, F_1, and F_2) and optical (D_3, E_3, and F_3) images of representative WS_2 supertwisted spirals with various twist angles grown around WO_x particles on SiO_2/Si substrates.

When a vdW crystal grows on such cone surfaces, it needs to maintain the angles between the edges as required by its Euclidean lattice. Meanwhile, it will also be bent following the curvature of the cone. Therefore, a 2D vdW crystal with a screw dislocation will grow into a supertwisted spiral shape, with a consistent twist angle of α between each successive layer (Fig. $1A_2$ and fig. S1B). Because the twist originates from the geometric mismatch between the non-Euclidean surface and Euclidean lattice, we name this phenomenon "non-Euclidean twist" and refer to the resulting twisted multilayered structures as "twisted superstructures" or "supertwisted spirals" (versus minute Eshelby twists) in the following discussion.

We can further describe the shape of these supertwisted spirals using a simple analytic geometry method. We can define two polar coordinates: (i) on the cone surface ($r_{c.s.}$, $\theta_{c.s.}$), and (ii) on the top-down projection of the cone surface ($r_{proj.}$, $\theta_{proj.}$). Therefore, the cone surface can be mapped to the projection by

$$\begin{cases} r_{\text{proj.}} = k r_{\text{c.s.}} \\ \theta_{\text{proj.}} = \dfrac{\theta_{\text{c.s.}}}{k} \end{cases}$$

where $k = 1 - \alpha/2\pi$ is the ratio between the angle of a "full circle" enclosing the cone center to the angle of a full Euclidean circle (2π, 360°). When k = 1, the surface is flat (Euclidean), resulting in an aligned spiral (Fig. $1C_1$), as discussed above. When k < 1, the surface is a cone, with its angular period (2π − α) less than the lattice period (2π). Therefore, each full lattice period carries an extra angle of α over into the total twist angle (fig. S2B). Thus, a cone surface transforms an aligned spiral into a "fastened" spiral (Fig. $1C_2$; the perspective view is shown in fig. $S1B_2$), like a fastened spiral torsion spring (movie S2). When k > 1, the surface is a developable "hyperbolic cone" surface (*31*) (Fig. $1C_3$). Because the lattice period (2π) is smaller than the angular period of such surface (2π − α, where α is negative) and cannot fill up space, an extra angle −α needs to be taken from the next lattice period (fig. S2C). Thus, a developable hyperbolic cone surface transforms an aligned spiral into an "unfastened" spiral (Fig. $1C_3$), like an unfastened spiral torsion spring (movie S3). In all three cases, α (either zero, positive, or negative) is the twist angle between successive layers. (See fig. S2 and associated discussion for our suggestion on naming different handedness levels of supertwisted spirals.)

Therefore, screw dislocations and non-Euclidean surfaces cooperate to create twisted superstructures of vdW crystals: First, the weak vdW interaction allows "movement" between layers; second, screw dislocations continuously generate "new layers" and maintain their relative orientations to the old ones (*22*); and third, the mismatched angular periods between non-Euclidean surfaces and Euclidean lattices provides an extra lattice twist (α) for every successive period in a continuous and consistent way. Using the equations derived above, we simulate the shapes of a series of twisted superstructures of right-handed screw-dislocation spirals with increasing positive or negative twist angles (Fig. 2A and fig. S3). We constrain the boundaries of layers so that the upper layers cannot go over the lower-layer edges. The envelopes of the twisting edges can be mathematically proven to be Archimedean curves. Even though the supertwisted spiral shapes with opposite twist angles appear very similar, they are not mirror images of each other, because they all have right-handed screw dislocations (and different substrate geometries). This non-Euclidean twist mechanism is also completely different from the lattice Eshelby twist mechanism for nanowires of vdW materials (*15*, *16*). In the Eshelby twist mechanism, the direction of the lattice twist is always the same as the screw dislocations, and

the twist angle (α) is determined by $\alpha = b/\pi r^2$, where b is the magnitude of screw dislocation and r is the nanowire radius, so that the twist angle is rather minimal at large radii (*14*). The non-Euclidean twist, however, can have either the same or opposite direction as that of a screw dislocation, which is determined by the type of non-Euclidean substrate surface (Fig. 1, C_2 and C_3). Moreover, the twist angle can be tunable over a wide range and is exclusively determined by substrate geometry in theory, regardless of the size of the 2D crystals, which allows them to scale up to any lateral dimension.

Although the non-Euclidean twist mechanism is mathematically illustrated on an infinitely large cone or developable hyperbolic cone surfaces, practically we can realize it on a flat substrate modified with suitable geometric features, on which only the center of a layered crystal spiral is affected by the non-Euclidean twist to continuously generate supertwisted layers. Once the initial orientation of a layer is set by its nucleus, the layer continues to grow along the same direction owing to the translational symmetry of the crystal lattice. Figure 2B shows three possible situations: (i) A flat substrate surface yields an aligned spiral without any twist (Fig. $2B_1$), (ii) a protruded substrate where the center of a screw dislocation sits on the center of a protrusion results in a fastened supertwisted spiral (Fig. $2B_2$), and (iii) a protruded substrate where the center of a screw dislocation sits on the edge of a protrusion leads to an unfastened supertwisted spiral (Fig. $2B_3$).

We have experimentally demonstrated the growth of such supertwisted spirals of WS_2 and WSe_2 on SiO_2/Si substrates (Fig. 2, D to F, and figs. S4 and S5) using a water vapor–assisted chemical vapor transport growth, with MX_2 as precursors and water vapor as the transport reagent (see methods for details) (*32*). As a comparison, Fig. 2C shows "normal" aligned triangular spirals with parallel edges. Such parallel edges rule out the Eshelby twist mechanism as the cause of twisted superstructures in these large pyramid-shaped spirals. The key to achieving non-Euclidean twists is to introduce protrusions onto substrates, as discussed above (Fig. 2, B_2 and B_3). Therefore, we drop-cast SiO_2 (200-nm diameter) or WO_3 (<100-nm diameter) nanoparticles onto SiO_2/Si substrates before the growth reactions (figs. S6 to S8). Intentional introduction of nanoparticles results in a proliferation of supertwisted spirals on typical growth substrates even though not every object is twisted. We also found that the reaction can spontaneously produce some WO_x particle side products (*32*, *33*) that can occasionally serve as the protrusions leading to the spontaneous growth of supertwisted spirals (figs. S9 and S10), but this process is much less reproducible. Because the formation mechanism is generally the same, we will ignore the difference between SiO_2, WO_3, and spontaneous formation in the subsequent discussion and only focus on understanding the geometric features of these supertwisted spirals.

Under an optical microscope, unlike the simple triangular shapes of aligned spirals (Fig. $2C_3$), the supertwisted spirals display circular or spiral shapes (Fig. 2, D_3, E_3, and F_3) that help us to rapidly spot them when the synthesis yield is low. The circular shape consists of three Archimedean spiral curves that result from the envelope curves of the three sets of edges (Fig. 2, D_2 and D_3), which is a good indication of the twisted superstructures. Detailed atomic force microscopy (AFM) imaging on the centers of these representative objects (Fig. 2, D_1, E_1, and F_1) reveals stacks of layers continuously twisting with a consistent twist angle from one layer to the next. Such a twist angle increases from Fig. 2, C to F, resembling the simulations shown in Fig. 2A. In fig. S4, a collection of 30 examples of supertwisted spirals of WS_2 or WSe_2 are characterized by optical microscopy and AFM, although not every object can be easily resolved with a simple structure model. Their specific morphologies vary with the different twist angles, the number of screw dislocations, and the stacking orders of MX_2 layers (figs. S3 and S11). Notably, Fig. 2, D_1, E_1, and F_1, as well as all AFM images in fig. S4, invariably reveals some particles, protrusions, or abnormality near the centers of the superstructures.

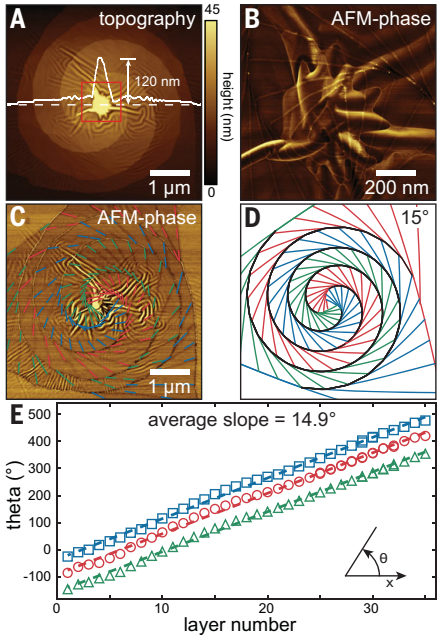

Fig. 3. Twist-angle evolution of a supertwisted WS_2 spiral. (**A**) Topography of a representative supertwisted spiral. The height profile along the horizontal dashed line reveals the height and width of the protrusion feature at the center. (**B**) Phase image collected from the red boxed area in (A) reveals wrinkles and layer edges at the spiral core. (**C**) Phase image corresponding to (A) with all the edges highlighted by colored dashed lines. (**D**) A supertwisted spiral simulated with a 15° twist angle with its edges highlighted. (**E**) Scatter plot of the evolving edge angles in (C) as a function of layer number counted from the bottom of the spiral to the top of the spiral. The least-squares linear fittings of each edge set (dashed lines) yield an average slope of 14.9° per layer. The colors of the data points correspond to the colors in (C).

We further verify the proposed non-Euclidean twist mechanism by examining the protrusion near the center and studying the relationship between the angles of edges and the layer numbers using a representative supertwisted WS_2 spiral grown on top of a SiO_2 particle (Fig. 3). The overall superstructure displays three sets of right-handed Archimedean spirals. The protrusion caused by the SiO_2 particle in the center is about 120 nm in height and 500 nm in diameter (Fig. 3A), forming a cone shape owing to the deformation of SiO_2 nanoparticles at the growth temperature around 1000°C (fig. S6; see cross-sectional scanning electron microscopy images in fig. S7). The wrinkles around the center (Fig. 3B) are formed as a result of the curvature difference when the WS_2 layers transit from the protrusion to the flat substrate. Despite these wrinkles, the orientations of all WS_2 layers are well preserved away from the center, likely owing to the strain tolerance of 2D crystal growth (*34*). The twisted layer edges can be better visualized with AFM phase contrast (Fig. 3B), which clearly reveals a right-handed screw dislocation. In Fig. 3C, all edges revealed by the AFM phase image are highlighted with colored dashed lines, and their angles are plotted as a function of layer number from the bottom of the spiral to the top of the spiral in Fig. 3E. We found an approximately linear relationship between the angle and layer number for all three "Archimedean arms," and linear fittings yielded an average twist of 14.9° per layer. The simulated supertwisted spiral using a 15° twist angle (Fig. 3D) matches the experimental morphology (Fig. 3C) very well. A similar twist angle analysis was carried out on a more complex supertwisted spiral of bilayers (fig. S12).

Furthermore, we carried out scanning transmission electron microscopy (STEM) analysis on a relatively thin and simple twisted WS_2 superstructure (Fig. 4) to characterize the moiré patterns expected in these twisted superstructures. (An idealized schematic illustration is shown in fig. S13.) Low-resolution high-angle annular dark-field (HAADF) imaging of the whole structure reveals the layer edges (Fig. 4A). A 4D STEM dataset collected on each layer

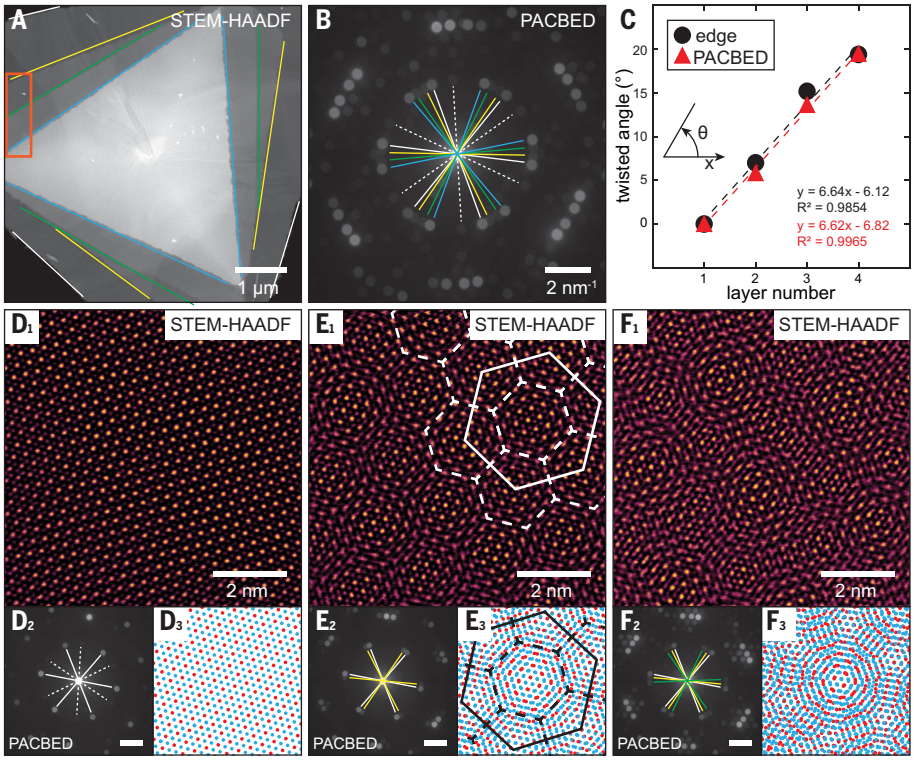

Fig. 4. STEM characterization of a non-Euclidean twisted superstructure. (**A**) HAADF image of a supertwisted WS_2 plate with edges of different layers highlighted by different colors. (**B**) Overall PACBED collected from the red boxed region in (A). The orientation of a specific layer can be measured by measuring the angle of a pair of diffraction disks from that layer. (**C**) Twist angles measured by morphology and diffraction as functions of the layer number, showing highly correlated linear relationships. The lattice angles are measured from six sets of diffraction disks, whereas the morphological twist angles are measured from three edges. R^2, coefficient of determination of linear regression. (**D_1**, **E_1**, and **F_1**) High-resolution HAADF images collected from the one-, two-, and three-layer areas in the red rectangular region in (A). The images were high-pass filtered for better visualization. (**D_2**, **E_2**, and **F_2**) PACBED collected from areas corresponding to (D_1, E_1, and F_1). Scale bars are 2 nm^{-1}. (**D_3**, **E_3**, and **F_3**) Simulated moiré patterns corresponding to (D_1, E_1, and F_1) using WS_2 models (W atoms, red dots; S atoms, blue dots).

(Fig. 4B) shows the position-averaged convergent beam electron diffraction (PACBED) pattern from the acquisition region, with lines marking diffraction spots attributed to each layer (fig. S14). Lattice twist angles are measured from the diffraction spots in Fig. 4B and plotted in Fig. 4C together with the morphological twist angle measured from Fig. 4A, showing that they match well. The twist angles increase linearly with the layer numbers at an average of 6.6° per layer. Atomic resolution HAADF images (Fig. 4, D_1, E_1, and F_1) acquired from the one-, two-, and three-layer regions show clear moiré patterns. The corresponding PACBED patterns from the same regions with a different layer number (Fig. 4, D_2, E_2, and F_2) clearly show different sets of diffraction disks from different layers. We also constructed the expected moiré patterns by overlapping multiple WS_2 models (Fig. 4, D_3, E_3, and F_3) with lattice rotations determined from diffractions, which match the observation well. Characterization of a more complicated superstructure (fig. S15) leads to similar findings. In addition, we also performed preliminary reflection spectroscopy and second-harmonic generation imaging to examine the inversion symmetry in supertwisted spirals (fig. S16).

We show how to generate continuously twisted superstructures of layered vdW materials by combining screw-dislocation spirals with non-Euclidean surfaces. By using nanoparticles as protrusions on flat substrates, we can introduce non-Euclidean surfaces to the growth process and experimentally demonstrate the direct growth of supertwisted spirals of WS_2 and WSe_2 materials with a wide range of twist angles and observed moiré patterns in STEM. More precise control of twist angles could be realized using nanofabricated substrates in the future.

REFERENCES AND NOTES

1. K. S. Novoselov, A. Mishchenko, A. Carvalho, A. H. Castro Neto, *Science* **353**, aac9439 (2016).
2. Y. Liu, Y. Huang, X. Duan, *Nature* **567**, 323–333 (2019).
3. F. Liu *et al.*, *Science* **367**, 903–906 (2020).
4. Y. Cao *et al.*, *Nature* **556**, 43–50 (2018).
5. K. L. Seyler *et al.*, *Nature* **567**, 66–70 (2019).
6. K. Tran *et al.*, *Nature* **567**, 71–75 (2019).
7. C. Jin *et al.*, *Nature* **567**, 76–80 (2019).
8. E. M. Alexeev *et al.*, *Nature* **567**, 81–86 (2019).
9. Y. Cao *et al.*, *Nature* **556**, 80–84 (2018).
10. G. Chen *et al.*, *Nat. Phys.* **15**, 237–241 (2019).
11. F. Wu, R.-X. Zhang, S. Das Sarma, *Phys. Rev. Research* **2**, 022010 (2020).
12. E. Khalaf, A. J. Kruchkov, G. Tarnopolsky, A. Vishwanath, *Phys. Rev. B* **100**, 085109 (2019).
13. T. Cea, N. R. Walet, F. Guinea, *Nano Lett.* **19**, 8683–8689 (2019).
14. M. J. Bierman, Y. K. A. Lau, A. V. Kvit, A. L. Schmitt, S. Jin, *Science* **320**, 1060–1063 (2008).
15. Y. Liu *et al.*, *Nature* **570**, 358–362 (2019).
16. P. Sutter, S. Wimer, E. Sutter, *Nature* **570**, 354–357 (2019).
17. C. Giacovazzo *et al.*, *Fundamentals of Crystallography*, C. Giacovazzo, Ed. (Oxford Univ. Press, ed. 2, 2002).
18. M. J. Greenberg, *Euclidean and Non-Euclidean Geometries: Development and History* (Macmillan Learning, 2007).
19. K. Liu *et al.*, *Nat. Commun.* **5**, 4966 (2014).
20. C.-C. Lu *et al.*, *ACS Nano* **7**, 2587–2594 (2013).
21. F. Meng, S. A. Morin, A. Forticaux, S. Jin, *Acc. Chem. Res.* **46**, 1616–1626 (2013).
22. M. J. Shearer *et al.*, *J. Am. Chem. Soc.* **139**, 3496–3504 (2017).
23. S. A. Morin, A. Forticaux, M. J. Bierman, S. Jin, *Nano Lett.* **11**, 4449–4455 (2011).
24. R. Y. Tay *et al.*, *Chem. Mater.* **30**, 6858–6866 (2018).
25. H. J. Park *et al.*, *Nano Lett.* **19**, 4229–4236 (2019).
26. L. Zhang *et al.*, *Nano Lett.* **14**, 6418–6423 (2014).
27. X. Fan *et al.*, *Nano Lett.* **18**, 3885–3892 (2018).
28. A. Zhuang *et al.*, *Angew. Chem. Int. Ed.* **53**, 6425–6429 (2014).
29. J. Dong, L. Zhang, F. Ding, *Adv. Mater.* **31**, e1801583 (2019).
30. S. Izumiya, M. C. Romero Fuster, M. A. S. Ruas, F. Tari, *Differential Geometry from a Singularity Theory Viewpoint* (World Scientific, 2014), p. 384.
31. S. M. Farmer, C. R. Calladine, *Int. J. Mech. Sci.* **47**, 509–520 (2005).
32. Y. Zhao, S. Jin, *ACS Materials Lett.* **2**, 42–48 (2020).
33. P. K. Sahoo, S. Memaran, Y. Xin, L. Balicas, H. R. Gutiérrez, *Nature* **553**, 63–67 (2018).
34. K. Wang *et al.*, *Sci. Adv.* **5**, eaav4028 (2019).
35. Z. Yuzhou, Yuzhou-Zhao/super-twisted-spirals: Super twisted spirals. Zenodo (2020); http://doi.org/10.5281/zenodo.3967881.
36. Y. Zhao, C. Zhang, P. M. Voyles, S. Jin, Supertwisted spirals of layered materials enabled by growth on non-Euclidean surfaces. Materials Data Facility (2020); http://doi.org/10.18126/M8UGYRK1.

ACKNOWLEDGMENTS

We thank B. Wang for helpful suggestions regarding the discussion of geometry. **Funding:** This research is support by the U.S. Department of Energy, Office of Basic Energy Sciences, Division of Materials Science and Engineering, under award DE-FG02-09ER46664 to S.J., J.C.W., Y.Z., D.D.K., and J.M.S. P.M.V. and C.Z. were supported by the U.S. Department of Energy, Office of Basic Energy Sciences, Division of Materials Science and Engineering, under award DE-FG02-08ER46547. We acknowledge the facilities supported by the UW-Madison Materials Research Science and Engineering Center (DMR-1720415). **Author contributions:** Y.Z. and S.J. conceived the idea and designed the experiments. Y.Z. performed the simulation, synthesis, AFM characterizations, STEM sample preparation, and data analysis. C.Z. and P.M.V. performed the focused ion beam milling, STEM characterizations, and analysis. D.D.K., J.M.S., and J.C.W. performed spectroscopy measurement and analysis. Y.Z. and S.J. wrote the paper with input from all authors. **Competing interests:** The authors declare no competing interests. **Data and materials availability:** All data are available in the main text or the supplementary materials. Computer codes for simulating supertwisted spiral shapes are available at Zenodo (*35*). 4D STEM data and averaged PACBED data are available through the Materials Data Facility (*36*).

SUPPLEMENTARY MATERIALS

science.sciencemag.org/content/370/6515/442/suppl/DC1
Materials and Methods
Figs. S1 to S16
References (*37*–*41*)
Movies S1 to S3

8 May 2020; accepted 2 September 2020
10.1126/science.abc4284

Supertwisted spirals of layered materials enabled by growth on non-Euclidean surfaces

Yuzhou Zhao, Chenyu Zhang, Daniel D. Kohler, Jason M. Scheeler, John C. Wright, Paul M. Voyles and Song Jin

Science **370** (6515), 442-445.
DOI: 10.1126/science.abc4284

Using curves to make twists

The growth of layered materials on flat substrates usually occurs in stacked layers, although defects or a lattice mismatch can induce strains that distort the shape of subsequent layers. However, these effects are usually small and can be uncontrolled. Zhao *et al.* now demonstrate the possibility of synthesizing multilayers of two-dimensional materials with certain twists between the layers induced by the presence of screw dislocations in combination with curved substrate surfaces. Different twist angles are achieved by varying the amount of nonplanarity and the character (conical or hyperbolic) of the surface.

Science, this issue p. 442